






Double-superradiant cathodoluminescenceAlexey Gorlach ^{1,*}, Ori Reinhardt ^{1,*}, Andrea Pizzi ^{2,3,*}, Ron Ruimy ¹, Gefen Baranes,^{1,3,4}
Nicholas Rivera,^{3,4} and Ido Kaminer ¹¹*Department of Electrical Engineering and Solid State Institute, Technion–Israel Institute of Technology, 32000 Haifa, Israel*²*Cavendish Laboratory, University of Cambridge, Cambridge CB3 0HE, United Kingdom*³*Department of Physics, Harvard University, Cambridge, Massachusetts 02138, USA*⁴*Department of Physics, Massachusetts Institute of Technology, Cambridge, Massachusetts 02139, USA*

(Received 26 August 2022; accepted 26 January 2024; published 28 February 2024)

There exist two families of superradiance phenomena: relying on free electrons or on correlated emission by ensembles of atoms. Here we investigate emission from ensembles of atoms driven by coherently shaped free electrons. This interaction creates superradiance emerging from both the atoms' and the electrons' coherence—with emission intensity that scales quadratically in both the number of atoms and number of electrons. This phenomenon enables electrons to become probes of quantum correlations in matter, with high temporal and spatial resolution.

DOI: [10.1103/PhysRevA.109.023722](https://doi.org/10.1103/PhysRevA.109.023722)**I. INTRODUCTION**

Electron microscopy is ubiquitous in imaging and spectroscopy of matter [1–3]. Recent advances propose using temporal [4–6] and spatial electron shaping [7–9] to affect electron-matter interactions, such as cathodoluminescence, which is the emission of light by free electrons impinging on matter [10–16]. Cathodoluminescence is central in modern electron microscopy, providing detailed information on optical properties of samples. The idea that cathodoluminescence can be enhanced by shaped electrons has received a recent burst of interest [17–26].

At the core of our understanding of enhanced cathodoluminescence by shaped electrons is the coherent interaction between a single two-level system and shaped free electrons. This interaction was first investigated using a semiclassical theory [17,18], proposing coherent control of the two-level system and enhancement of cathodoluminescence [17]. Soon after, the fully quantum regime of this interaction was revealed [19–21,25], leading to unique possibilities for imaging the coherent state of matter [20], resolving the wave function of the emitting free electrons [23], and performing homodyne-type measurements [24]. In all these works, the enhanced electron-matter interaction scales quadratically in the number of electrons, similar to the phenomenon of electron superradiance [27–33]. Electron superradiance describes the constructive interference in the radiation field or near field of multiple electrons, when they are phase locked to each other. This type of superradiance is the source of coherent radiation in celebrated examples such as free-electron lasers [32], klystrons [31], synchrotrons [27–29], and certain Smith-Purcell sources [30].

Atomic Dicke superradiance, which differs from electron superradiance, is the collective radiation by multiple excited atoms that exhibits faster rates of spontaneous emission compared to individual atoms [34,35]. Throughout the paper, we use the word “atom” to refer to any emitter from which superradiance can occur, including actual atoms, molecules, and quantum dots. Atomic superradiance plays an important role in quantum optics [36,37], relativity [38], astrophysics [39], and condensed matter [40]. However, atomic superradiance has never been considered in the context of cathodoluminescence. It remains unknown how the superradiant atomic system interacts with free electrons and whether atomic correlations can additionally enhance cathodoluminescence.

Here we consider the interaction of shaped electrons with a many-body system, finding an interplay of atomic and electron superradiance, which results in a drastic enhancement of cathodoluminescence. We present a quantum theory of the interaction between an ensemble of N_a atoms and N_e free electrons, capturing the effect of free-electron-induced superradiance (Fig. 1). Depending on whether the atoms are in the superradiant state or not, and whether the free electrons are shaped or not, we identify four possible regimes of cathodoluminescence, with emission intensity I scaling as $N_a N_e$, $N_a N_e^2$, $N_a^2 N_e$, or $N_a^2 N_e^2$ [Figs. 1(a)–1(d)]. The last regime is the focus of this work. This regime occurs when the atoms emit coherently after excitation from shaped electrons, with an interplay of both electron- and atomic-superradiant effects. The superradiant phenomena happening here can be detected not only in the emission of light but also in the energy spectrum of the electrons, as discussed further in [41]. The preliminary results that led to our work here were presented in [42].

Let us discuss how the double-superradiant regime [Fig. 1(d)] arises. The shaped electrons interact with the atomic system coherently such that the excitations they induce accumulate in a coherent manner [17,20,21]. Thus, the total energy of the atomic system after the excitation by N_e

*These authors contributed equally to this work.

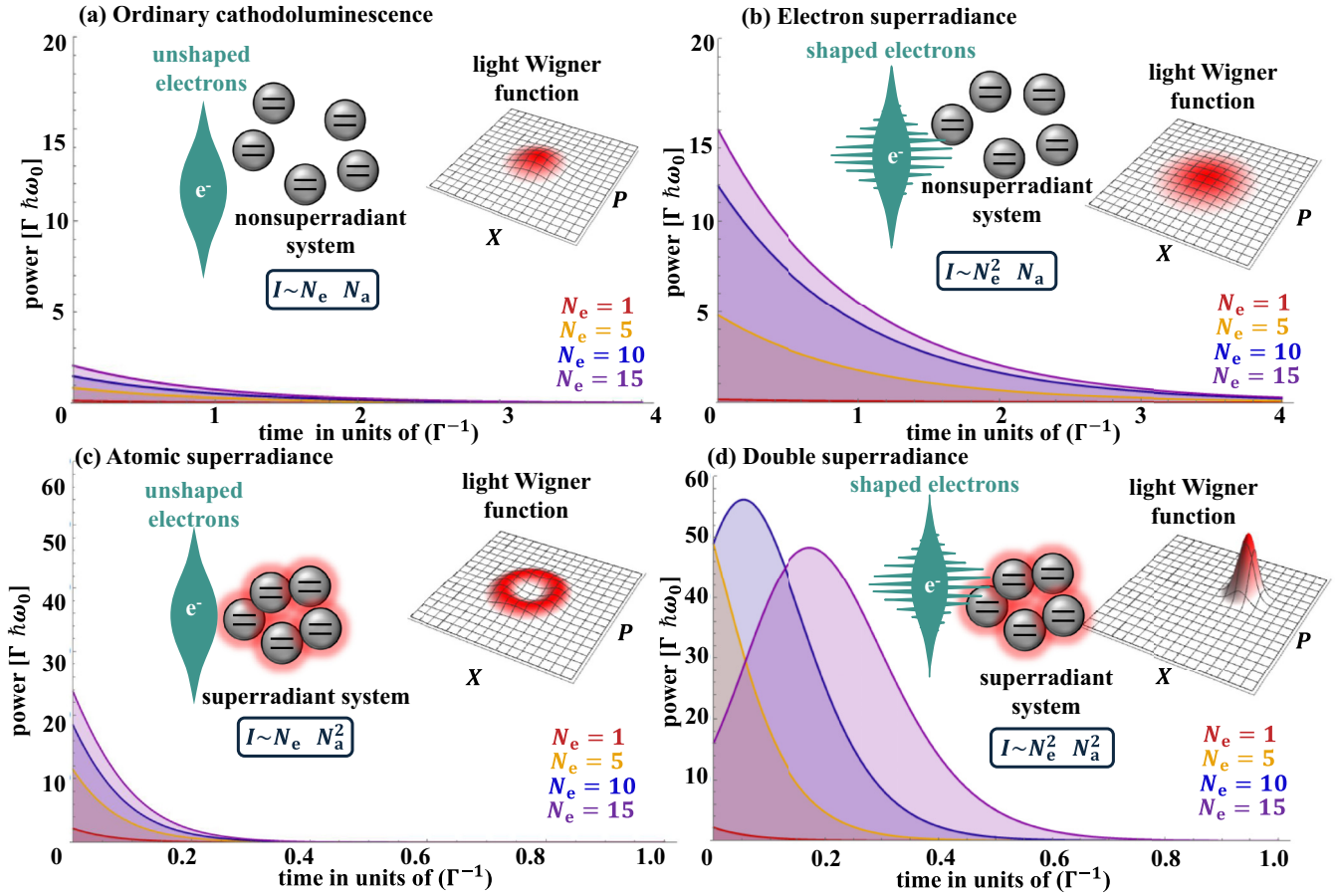


FIG. 1. Double-superradiant cathodoluminescence. (a,b) Emission intensity of the nonsuperradiant atomic system after the interaction with unshaped ($\sigma = 0.0$) and comb electrons ($\sigma = 3.0$), respectively. The emission intensity from a single electron ($N_e = 1$) does not depend on the electron shape. The atomic system is nonsuperradiant: the atoms are excited independently and are not in phase, leading to incoherent thermal emission. (c,d) Emission intensity of the superradiant atomic system after the interaction with unshaped ($\sigma = 0.0$) and comb electrons ($\sigma = 3.0$), respectively. The atomic emission from unshaped electron excitation has no phase, but the atoms are correlated. This leads to an incoherent Poissonian Wigner function of the emitted light. Comb electrons induce a coherent excitation. For a small number of comb electrons, the emission is a coherent state as shown in (d). However, a large number of comb electrons take the atomic system close to the fully excited state, and the emitted light gets close to a Fock state. The plots assume $g = 0.1$ and $N_a = 15$ [the coupling constant g is defined below after Eq. (3)]. Note: the Wigner functions shown here are schematic and for illustrative purposes only.

electrons will be proportional to N_e^2 . If we assume that the electrons have the same interaction with all the atoms, then the excited state is described by Dicke symmetric states [34]. The resulting collective emission follows the Dicke theory, with peak emission intensity proportional to N_a^2 instead of N_a for independent spontaneous emission when we keep the energy per atom fixed [35]. Indeed, the intensity of the superradiant emission is N_a times more intense compared to the case of independent spontaneous emission. Since the emission intensity depends on the initial excitation, we get both effects of atomic and electron superradiance being combined so that I scales as $N_a^2 N_e^2$. We note that the lifetime of the emission pulse strongly depends on the number of atoms N_a (according to Dicke's theory of superradiance), but is only weakly affected by the number of electrons N_e since the lifetime is independent of the energy in the case of a perfectly symmetric excitation.

The shaping of electrons discussed in this work is possible thanks to the recent advances in ultrafast electron microscopy

experiments, and specifically the advent of photon-induced near-field electron microscopy (PINEM) [2,4,5,43–48].

II. INTERACTION BETWEEN FREE ELECTRONS AND A MANY-BODY ATOMIC SYSTEM

In this section, we develop the theory of the interaction between free electrons and an ensemble of atoms. We model each atom as a two-level system, which is the standard approach for the description of both the electron-atom interaction [17,20–22] and superradiance [34]. We assume that before the interaction with electrons all atoms are in the ground state. We should note that the electron can undergo multiple competing transitions including excitations of core levels in the atoms and emission of bremsstrahlung [49] (elaborated upon in [20]). These competing transitions occur with smaller probabilities for shaped electrons as the shaping makes the interaction resonant for the specific atomic transition that matches the shaping frequency [17]. Furthermore,

when looking at the cathodoluminescence signal, neglecting the competing transitions is even more relevant since the two-level emission is further enhanced by superradiance [34]. Achieving the conditions of superradiance requires having the

distance between atoms smaller than the wavelength of the emitted light and electron-atom interaction length.

We denote the ground and excited states of every single atom by $|g\rangle$ and $|e\rangle$. The Dicke symmetric states are

$$\begin{aligned} |0\rangle &\equiv |ggg \dots gg\rangle, \\ |1\rangle &\equiv \sqrt{1/N_a}(|egg \dots gg\rangle + |geg \dots gg\rangle + \dots + |ggg \dots ge\rangle), \\ &\dots \\ |N_a\rangle &\equiv |eee \dots ee\rangle. \end{aligned} \quad (1)$$

The Hamiltonian of a single electron interacting with the superradiant system (in analogy to [20]) reads

$$H = -i\hbar v \partial_z + \frac{\hbar\omega_0}{2} S_z + \frac{e\gamma}{4\pi\epsilon_0} \cdot \frac{(\mathbf{d}_\perp \cdot \mathbf{r}_\perp + d_\parallel z)S_+ + (\mathbf{d}_\perp^* \cdot \mathbf{r}_\perp + d_\parallel^* z)S_-}{(\gamma^2 z^2 + r_\perp^2)^{3/2}}. \quad (2)$$

The first two terms describe the Hamiltonians of the free electron and the superradiant system, respectively. $S_\pm = \sum_i (\sigma_i^x \pm i\sigma_i^y)$, $S_z = \sum_i \sigma_i^z$ are the symmetric operators, with $\sigma_i^{x,y,z}$ the Pauli operators of the i th atom. v is the average velocity of the electron, γ is the relativistic factor, and $\hbar\omega_0$ is the transition energy of the two-level atoms. The third term in Eq. (2) describes the interaction between the electron and the atoms with transition dipole moment \mathbf{d} , having the perpendicular \mathbf{d}_\perp and parallel d_\parallel components relative to the electron trajectory. The distance between the electron and the atoms is r_\perp ; the elementary charge is e and vacuum permittivity is ϵ_0 . Equation (2) is valid under the paraxial-electron approximation, which is justified in all relevant experiments (e.g., [1–3]), considering that typical electron energy values (~ 100 keV) are much larger than typical transition energies ($\hbar\omega_0 \sim 1$ eV).

Under the above conditions, we use the Magnus expansion (up to first order) [50] to describe the scattering matrix of the

interaction between one electron and the many-body atomic system;

$$U = e^{-i(gbS_+ + g^*b^\dagger S_-)}, \quad (3)$$

where b and b^\dagger are the electron energy shift operators, reducing and increasing the electron energy by quanta of $\hbar\omega_0$. g is a dimensionless coupling coefficient that according to [17,20] equals

$$g = \frac{ed_\perp\omega_0}{2\pi\epsilon_0\hbar\gamma v^2} K_1\left(\frac{\omega_0 r_\perp}{\gamma v}\right) + i \frac{ed_z\omega_0}{2\pi\epsilon_0\hbar\gamma^2 v^2} K_0\left(\frac{\omega_0 r_\perp}{\gamma v}\right).$$

The result in Eq. (3) is valid when $|g| \ll 1$, which describes all known practical situations.

We express the scattering matrix equation (3) in the symmetric states' basis:

$$\langle m|U|n\rangle \equiv b^{n-m} U_{mn},$$

$$U_{mn} = \sqrt{m!n!(N-n)!(N-m)!} \sum_{k=0}^n \frac{(-1)^k (\cos|g|)^{N-m+n-2k} (i \sin|g|)^{m-n} (\sin|g|)^{2k}}{k!(n-k)!(m-n+k)!(N-m-k)!}. \quad (4)$$

Considering all the atoms initially in their ground state, the postinteraction atomic density matrix after tracing out the electron is

$$\rho_f^{kl} = \sum_{m,n} \langle \psi_e | b^{(m-k)-(n-l)} | \psi_e \rangle U_{km} \rho_i^{mn} U_{nl}^\dagger, \quad (5)$$

where $|\psi_e\rangle$ is the wave function of the electron before the interaction. We emphasize that, by contrast with the standard case of a fully excited atomic ensemble, Eq. (5) accounts more generally for an atomic state with a different number of atoms excited (labeled by m).

Equation (5) provides the density matrix of the atoms after their interaction with a single electron of any *arbitrary* wave function $|\psi_e\rangle$. To show double superradiance [Figs. 1(c) and 1(d)], we apply Eq. (5) N_e times sequentially. Each iteration

obtains a new atomic density matrix that serves as the initial condition for the interaction with the next electron. This procedure is correct when the electron pulse duration and the electron-atoms interaction duration are much shorter than the superradiance time and the emitters coherence time T_2^* . To justify this assumption, consider typical pulses of $N_e = 10$ electrons in a duration of $\tau = 1$ ps, which is much shorter than even the faster superradiant times (e.g., $t \sim \Gamma^{-1} N_a^{-1} \sim 67$ ps, estimated for $N_a = 15$ atoms with an intrinsic lifetime

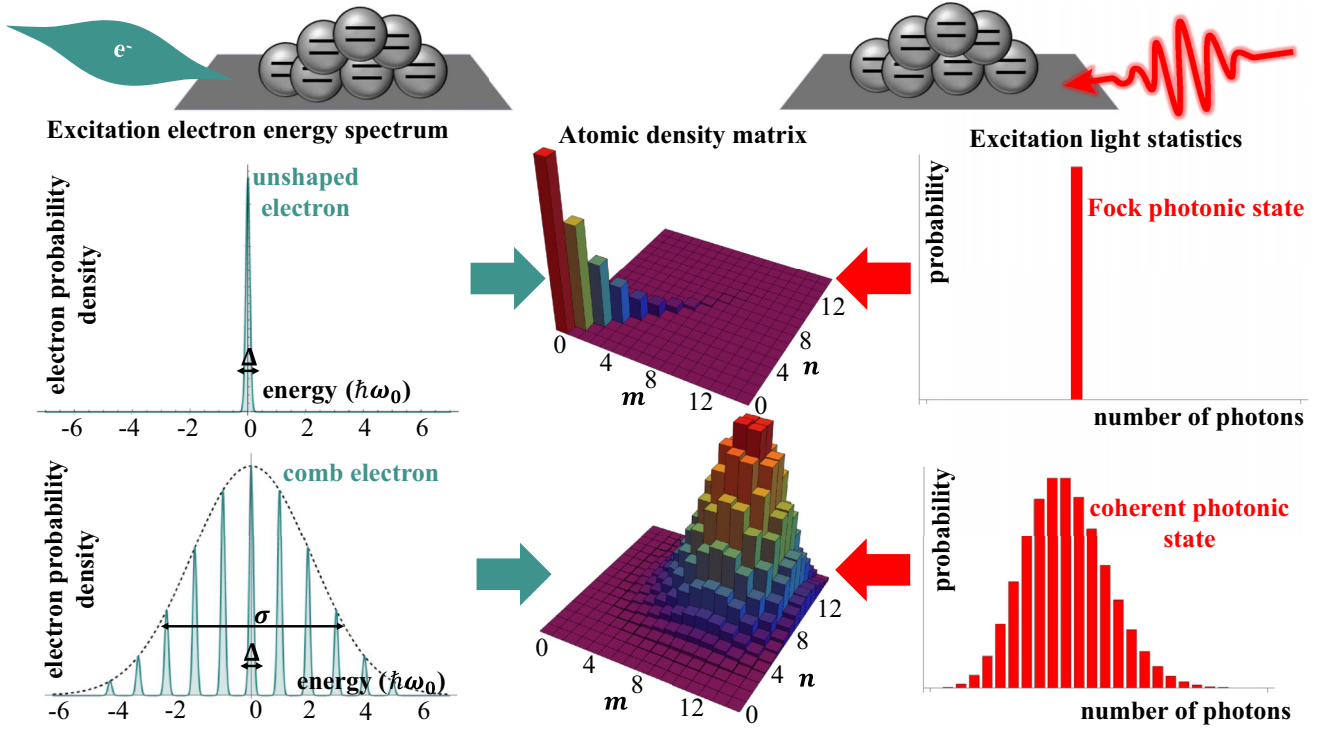


FIG. 2. Analogy between electron-driven and light-driven superradiance. The excitations of the superradiant atomic system by a Fock and a coherent light state are analogous to the excitations by an unshaped and a comb electron, respectively. This analogy is correct because unshaped free electrons and Fock states of light entangle with the atomic system, while comb electrons and coherent light do not entangle with the atomic system. In cases of entanglement, the atomic system loses its coherence after the interaction (diagonal density matrix, top row). In cases of no entanglement, the information about the phases between different atomic states remains unchanged after the interaction (off-diagonal elements in the density matrix, bottom row).

of $\Gamma^{-1} \sim 1$ ns). A theory able to capture effects beyond this assumption, accounting for many-electron states in a nonsequential fashion, remains an open challenge for future research.

III. EFFECT OF THE ELECTRON SHAPE ON THE MANY-BODY ATOMIC SYSTEM

We now show how the electrons' shape impacts the atomic state. The electrons' shaping is defined by the moments $\langle b^n \rangle$ (i.e., bunching factor [51]). The electron that has all $|\langle b^n \rangle| = 1$ has the most coherent interaction with atomic systems. To realize $|\langle b^n \rangle| \approx 1$, we need electrons of wide coherent energy uncertainty, or equivalently, comb electrons [52], made from a sequence of coherent energy peaks [53–55]. The phase of the wave function should scale linearly in energy (as created using established techniques [53,54]). Thus, we consider comb electron states such as

$$|\psi_e\rangle = \frac{1}{\sqrt{\text{norm}}} \sum_n e^{i\phi n} e^{-\frac{n^2}{2\sigma^2}} |\psi_n\rangle, \quad (6)$$

where $\phi \in [0, 2\pi]$ is an arbitrary phase, σ is the dimensionless comb bandwidth, and $|\psi_n\rangle$ is unshaped electron states with central energy $E_0 + n\hbar\omega$:

$$|\psi_n\rangle = \frac{1}{\sqrt{\text{norm}}} \int dE e^{-\frac{(E-E_0-n\hbar\omega)^2}{2\Delta^2(\hbar\omega)^2}} |E\rangle. \quad (7)$$

Here Δ is the dimensionless width of the unshaped electron (typically we have $\Delta < \hbar\omega$, e.g., in electron microscopy [1]). Normalization yields $\langle \psi_m | \psi_n \rangle = \delta_{mn}$. The input electrons in conventional electron microscopes, termed unshaped electrons, have $\sigma < 1$, and can be shaped into comb electrons with $\sigma \sim 3$ [53,54]. Much larger σ values were demonstrated [52,56], but without satisfying the linear-phase requirement. We will generally assume a resonance condition, $\hbar\omega = \hbar\omega_0$, meaning that the electrons match the frequency ω_0 of the transition for the two-level atoms. The effect of breaking such resonance condition is investigated later.

Figure 2 compares the atomic density matrix after interacting with unshaped ($\sigma < 1$) and shaped comb electrons ($\sigma \sim 3$). The effect of such interactions is analogous to excitations by a many-photon Fock state and a coherent state of light, respectively. Thus, the electrons can emulate excitations by quantum photonic states such as Fock states. The creation of such “electron Fock states” is much simpler than the creation of Fock light states (being the initial electron state from typical electron guns [1]).

Free electrons can be also used to control the postinteraction quantum state of the atoms, and in turn, the quantum state of the light subsequently emitted from the atoms (Wigner functions shown in Fig. 1). In Fig. 1(a), nonsuperradiant atoms emit incoherent light in ordinary cathodoluminescence. The emission is thermal and does not have a definite phase because of averaging over a large number of independent atoms. In

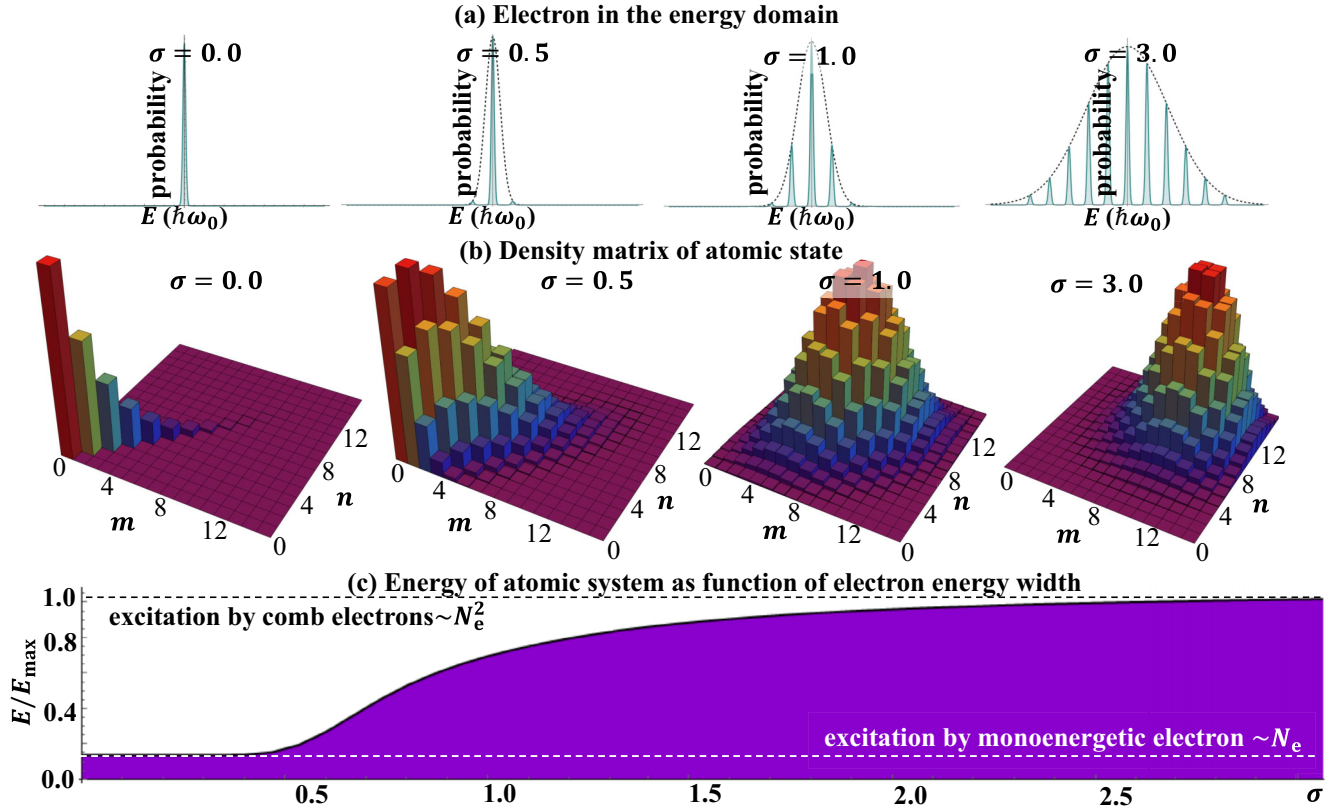


FIG. 3. The effect of electron shaping on inducing correlations between atoms. (a) The electron energy spectrum before the interaction for different energy bandwidths σ of the shaped electron. A wider bandwidth corresponds to stronger bunching. (b) The atomic density matrix after the electron interaction for different bandwidths σ . (c) The average atomic excitation energy following an interaction with N_e electrons as a function of their energy bandwidth σ . The narrow energy bandwidth electron excitation scales as N_e , while the wide energy bandwidth electron excitation scales as N_e^2 . In the limit of a perfect energy comb ($\sigma \rightarrow \infty$), the excitation energy is the largest possible and can be computed exactly (dashed line). Parameters are as in Fig. 1.

Fig. 1(b), the thermal emission can be enhanced by electron superradiance, but since the atoms are still independent, the light emission phase remains random. In Fig. 1(c), superradiant atoms emit light with Poissonian statistics and uncertain phase when driven by unshaped electrons. The uncertainty in the phase of the emission is caused by the entanglement between unshaped electrons and atoms.

In Fig. 1(d), in contrast with the above, only the superradiant emission triggered by shaped electrons creates coherent states of light with a fixed phase. This phase is then locked to the shaped electrons' phase. For a weak excitation, the emitted light will be mostly in a coherent state, whereas for a fully excited state the emitted light will be close to a Fock state.

The case of a single electron interacting with a superradiant atomic system is also a particular case of Fig. 1(d), as long as the electron is preshaped. In this case, the emission will have a certain phase, but without electron superradiance since $N_e = N_e^2 = 1$. Similarly, the interaction of multiple shaped electrons with a single atom will cause the emission of a coherent state, but without atomic superradiance since $N_a = N_a^2 = 1$.

The same effects described here for a (*quantum*) comb electron wave function are also relevant for (*classical*) bunched electrons, whose classical temporal distribution is analogous to the wave function shape. The classical interaction time is similarly related to the comb electron's phase ϕ [from Eq. (6)], determining the phase of the emitted light. Thus, the word "shaping" applies both to the quantum wave function and classical distribution. Curiously, this is a problem for which, thanks to its discrete nature, the quantum description of the electron-atom interaction is simpler than the classical one, and thus preferable.

The influence of the electron bandwidth σ (or bunch width) on the postinteraction atomic state is shown in Fig. 3. The probability of the atoms' excitation increases (by N_e) for broader electron energy envelopes [Fig. 3(a)]. A similar classical-quantum correspondence appears in electron-light interactions, which also depend on the electron energy bandwidth [57].

The average excitation energy of the atomic system after an interaction with N_e electrons reads (details in the Appendix)

$$\langle E \rangle = N_a \frac{(\lambda_+^{N_e} - \lambda_-^{N_e})(1 - \langle b^2 \rangle) |\sin |g|| - (\lambda_+^{N_e} + \lambda_-^{N_e} - 2) \sqrt{(1 - \langle b^2 \rangle)^2 \sin^2 |g| - 16 \langle b \rangle^2 \cos^2 |g|}}{4 \sqrt{(1 - \langle b^2 \rangle)^2 \sin^2 |g| - 16 \langle b \rangle^2 \cos^2 |g|}}, \quad (8)$$

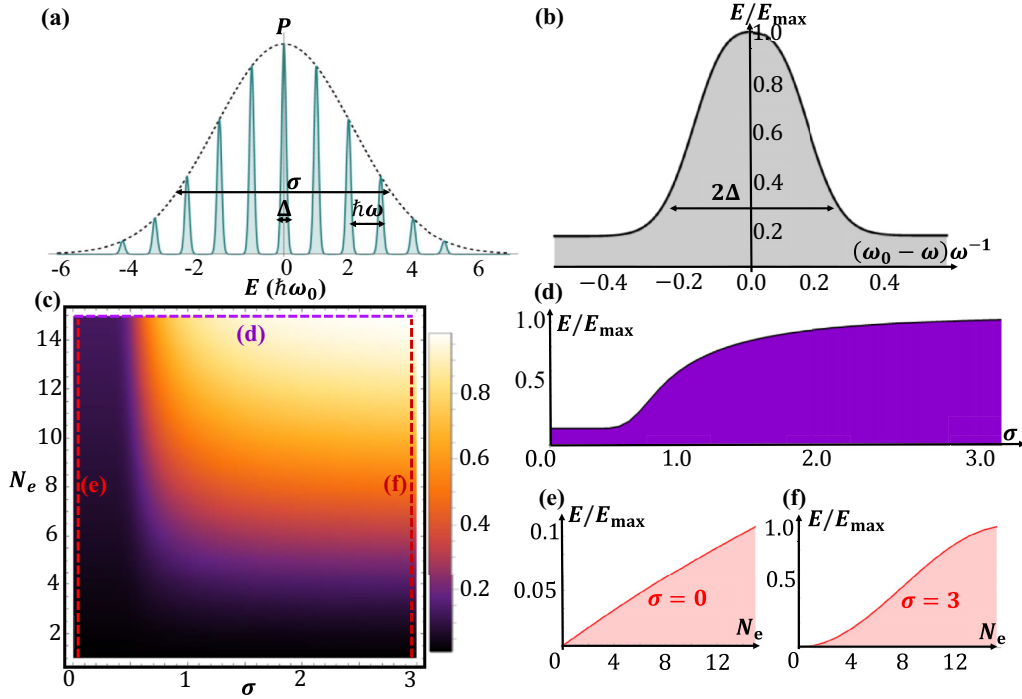


FIG. 4. Energy of excitation of the atomic system for a shaped electron. (a) The electron comb has energy width σ and is composed of many peaks of width Δ equispaced in energy by $\hbar\omega$. (b) Average energy E of the atomic system after the interaction with $N_e = 15$ comb electrons ($\sigma = 3$), as a function of the detuning between the atomic transition ω_0 and the energy period of the comb ω . The curve has a peak with width 2Δ . Therefore, the atoms' excitation will effectively occur even in the presence of detuning, as long as $|\omega_0 - \omega|/\omega \ll \Delta$ (in fact, atoms are excited even if the detuning is large, although less effectively). Thus, the two-level model that we are using for the emitters will be correct when the emitter's energy levels have more than Δ separation. The average energy is normalized to the maximal energy of the excitation $E_{\max} = N_a \hbar\omega_0$. (c) Average energy of the excitation as a function of the number of electrons N_e and width of the comb σ . We observe that comb electrons excite the system to much higher energies than the unshaped electrons do. (d) Average energy as a function of σ for fixed $N_e = 15$ [this plot corresponds to the purple line in (c)]. (e,f) Average energy as a function of N_e for two different widths $\sigma = 0$ and $\sigma = 3$, corresponding to the red lines in (c). These plots show that for unshaped electrons the excitation is proportional to N_e , while for comb electron the excitation energy is proportional to N_e^2 .

where

$$\lambda_{\pm} = \frac{1}{2}(3\cos^2|g| - 1 - \langle b^2 \rangle \sin^2|g|) \pm \sin|g| \sqrt{(1 - \langle b^2 \rangle)^2 \sin^2|g| - 16\langle b^2 \rangle \cos^2|g|}.$$

For unshaped electrons ($\sigma \ll 1$) we get $\langle E \rangle = \frac{N_a}{2}(1 - \cos^{N_e} 2|g|)$, which for a weak excitation $N_e|g| \ll 1$ approximates as $\langle E \rangle \approx N_a N_e |g|^2$. For an ideal comb ($\sigma \gg 1$), we get instead $\langle E \rangle \approx N_a \sin^2 N_e |g|$, which for a weak excitation approximates as $\langle E \rangle \approx N_a N_e^2 |g|^2$. That is, the atomic excitation energy scales as N_e for unshaped electrons and as N_e^2 for comb electrons. The full numerical evaluation of Eq. (8) is shown in Fig. 4.

IV. FREE-ELECTRON-INDUCED SUPERRADIANT EMISSION

To analyze the superradiance by the atomic system, we note that the electrons (shaped or unshaped) excite only sym-

metric states. Due to the short atoms-electrons interaction duration (typically < 1 ps), we can split the dynamics into two sequential steps: (1) calculate the atomic density matrix after the interaction with N_e electrons according to Eq. (5); then (2) use this density matrix as the initial condition for a conventional calculation of Dicke superradiance [34–36].

The following calculation can be used to analyze both electron-driven and light-driven superradiance. We should emphasize that here “driven” and “induced” refer to the initial atom excitation stage, whereas the consequent emission is then spontaneous. Let us call $\rho(0)$ the postinteraction atomic density matrix, as obtained from Eq. (5). The time evolution of the atomic density matrix during the superradiance is given by [34–36]

$$\frac{d\rho^{mn}(t)}{dt} = -\frac{\Gamma(m(N-m+1) + n(N-n+1))\rho^{mn}(t)}{2} + \Gamma\sqrt{(m+1)(N-m)(n+1)(N-n)}\rho^{(m+1)(n+1)}(t), \quad (9)$$

where Γ is the rate of spontaneous emission of an individual atom. The emission intensity is obtained through energy conservation as

$$I = -\frac{d}{dt} \left(\frac{\hbar\omega_0}{2} \langle S_z \rangle \right) = -\hbar\omega_0 \sum_{m=0}^N m \frac{d\rho^{mm}(t)}{dt}. \quad (10)$$

Beyond the intensity, we can characterize quantum correlations of the emitted light using the model developed in [36,37], and generalized to yield the full Wigner function [58,59]. We use this development to show the Wigner function of the emitted light in Fig. 1.

V. DISCUSSION

We expect the phenomenon of double superradiance to be accessible in current experimental setups. Specifically, promising candidate setups are quantum dot platforms in which atomic superradiance or superfluorescence have been reported when driven by light [60]. Driving these materials using shaped free-electron pulses could initiate the process we predict above. Such an observation would access the hard-to-reach coherent interaction between electrons and atoms or other types of quantum emitters.

Indeed, while the interactions between electrons and atoms are ubiquitous, e.g., in electron loss spectrometry and electron microscopy, these interactions are generally incoherent. The coherent interaction of electrons with atoms, in which the energies of the electrons and atoms are resonant and the phase of the electrons is imprinted on the atoms, offers exciting prospects. Previous theoretical works in this field (e.g., [17,20,21]) showed that the electron-atom interaction depends on the electrons' shape. However, this effect remained inaccessible experimentally because of the weak interaction (typical $|g| \sim 10^{-2} - 10^{-3}$) in realistic systems. The intensity of emission from individual atoms is similarly weak ($I \propto |g|^2 < 10^{-4}$). Double superradiance could resolve this challenge by enhancing the interaction by $N_a N_e$ times (e.g., 150 times for $N_a = 15$ and $N_e = 10$). Such enhancement can help surpass competing decoherence channels that so far prevented the observation of coherent electron-atom interactions.

Double superradiance may also help demonstrate the so far unobserved influence of electrons' shape on electron-atoms interactions. The strength of the interaction and the consequent emission depend on the shape as shown in Figs. 3 and 4. The shape also alters the quantum state of the emitted light (e.g., photon statistics), which can be extracted using quantum optical characterizations such as $g^{(2)}$ and homodyne measurements.

A proposal for the experimental implementation of double superradiance is illustrated in Fig. 5. The electrons are pre-shaped into an energy comb using interactions with intense laser light [53,54]. These shaped electrons then interact with the atomic system, inducing emission that is collected and analyzed to extract the classical time-dependent intensity of the emitted light, for example, using a streak camera. Quantum properties of the light such as its Wigner functions (Fig. 1) can be extracted, for example, using homodyne schemes that rely on a local oscillator based on the shaped electrons or on the

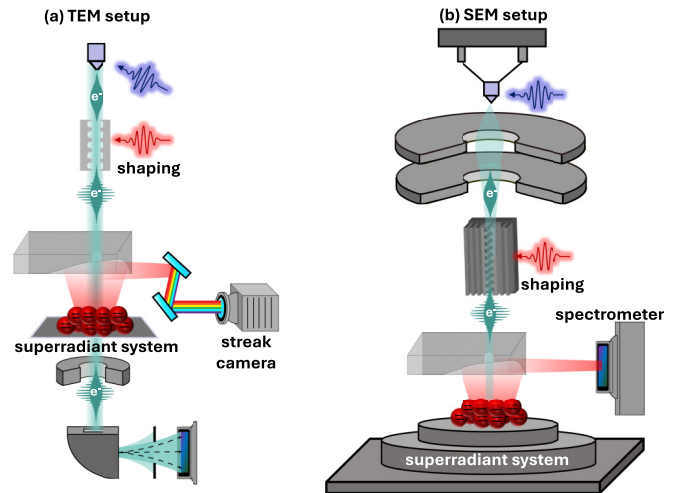


FIG. 5. Experimental schemes for measuring double-superradiant cathodoluminescence. Schematic setups of an ultrafast (a) transmission or (b) scanning electron microscope (TEM or SEM). A pulse of electrons can be photoinduced and shaped using a laser and a coupling structure, e.g., dielectric laser accelerator structures [61,62] or a set of mirrors [52]. Each shaped electron pulse excites an ensemble of atoms. The atoms then relax through superradiant emission, which can be collected and characterized in various ways, such as a streak camera for combined spectral and temporal information. The electrons' energy spectra can be simultaneously measured for additional information, as shown recently in [63,64].

laser that shaped them (as in [24]). Such experiments can be implemented in ultrafast (laser-driven) transmission or scanning electron microscopes—Figs. 5(a) and 5(b), respectively.

Looking forward, free electrons may become prime candidates to investigate superradiance with high spatial and temporal resolution beyond the limits enforced by conventional light excitations. The spatial resolution of light excitations is typically limited by the wavelength, i.e., hundreds of nanometers, making it impossible to selectively trigger superradiance in small regions of a target sample. By contrast, electrons enable triggering superradiance in selected small regions of the sample, thanks to their short de Broglie wavelength (down to a few nanometers in scanning electron microscopes and even to subnanometer in transmission electron microscopes).

The temporal resolution of resonant light excitations is typically limited to hundreds of femtoseconds because shorter pulses involve broader bandwidths that are mostly out of resonance for the intended transition. In contrast, electrons carry higher energies so they can have the broad energy bandwidth required for forming attosecond pulses [65] while maintaining a resonant excitation of the intended transition.

Altogether, we envision that using electrons instead of light could provide alternative methods to control many-body quantum systems. Double-superradiant cathodoluminescence can also give access to unique superradiance-related imaging capabilities, even for matter in nonequilibrium states.

APPENDIX

1. Interaction of an arbitrary electron state with a superradiant ensemble of atoms

The Hamiltonian of the interaction between a single two-level atom and an arbitrary electron state can be described by the following Hamiltonian (according to [20]),

$$H = -i\hbar v \partial_z + \frac{\hbar\omega_0}{2} \sigma_z + \frac{e}{4\pi\epsilon_0} \cdot \frac{(\mathbf{d}_\perp \cdot \mathbf{r}_\perp + d_\parallel z) \sigma_+ + (\mathbf{d}_\perp^* \cdot \mathbf{r}_\perp + d_\parallel^* z) \sigma_-}{(z^2 + r_\perp^2)^{\frac{3}{2}}}, \quad (\text{A1})$$

where the first two terms describe the Hamiltonians of the free electron and the two-level atom. The σ 's are the Pauli operators of the atom. v is the average velocity of the electron and $\hbar\omega_0$ is the energy of a two-level atom. The third term in Eq. (2) describes the interaction between the electron and the atoms with the transition dipole moment \mathbf{d} , composed of a component perpendicular, \mathbf{d}_\perp , and parallel, d_\parallel , to the electron's trajectory. The distance between the electron and the atom is r_\perp , the elementary charge is e , and vacuum permittivity is ϵ_0 .

Equation (A1) can be easily generalized to the case of a superradiant ensemble of atoms if we consider them in a volume small enough that they have the same coordinate:

$$H = -i\hbar v \partial_z + \frac{\hbar\omega_0}{2} S_z + \frac{e}{4\pi\epsilon_0} \cdot \frac{(\mathbf{d}_\perp \cdot \mathbf{r}_\perp + d_\parallel z) S_+ + (\mathbf{d}_\perp^* \cdot \mathbf{r}_\perp + d_\parallel^* z) S_-}{(z^2 + r_\perp^2)^{3/2}}, \quad (\text{A2})$$

where $S_\pm = \sum_i (\sigma_i^x \pm i\sigma_i^y)$, $S_z = \sum_i \sigma_i^z$ are the symmetric operators, with $\sigma_i^{x,y,z}$ the Pauli operators of the i th atom. We separate the Hamiltonian in Eq. (2) into two parts: the free Hamiltonian, $H_0 = -i\hbar v \partial_z + \frac{\hbar\omega_0}{2} S_z$, and the interaction Hamiltonian, $H_1 = \frac{e}{4\pi\epsilon_0} \cdot \frac{(\mathbf{d}_\perp \cdot \mathbf{r}_\perp + d_\parallel z) S_+ + (\mathbf{d}_\perp^* \cdot \mathbf{r}_\perp + d_\parallel^* z) S_-}{(z^2 + r_\perp^2)^{3/2}}$. Then in the interaction picture, the Hamiltonian has the following form:

$$V_1 = e^{\frac{iH_0 t}{\hbar}} H_1(t) e^{-\frac{iH_0 t}{\hbar}}.$$

This Hamiltonian can be simplified and takes the form

$$V_1(t) = \frac{e}{4\pi\epsilon_0} \cdot \frac{[\mathbf{d}_\perp \cdot \mathbf{r}_\perp + d_\parallel(z + vt)] S_+ e^{i\omega_0 t} + [\mathbf{d}_\perp^* \cdot \mathbf{r}_\perp + d_\parallel^*(z + vt)] S_- e^{-i\omega_0 t}}{[(z + vt)^2 + r_\perp^2]^{\frac{3}{2}}}. \quad (\text{A3})$$

The scattering matrix can be written in terms of the Magnus expansion [50],

$$U = \exp\left(\sum_{k=1}^{\infty} \Omega_k\right), \quad (\text{A4})$$

where

$$\begin{aligned} \Omega_1 &= -\frac{i}{\hbar} \int_{-\infty}^{+\infty} dt V_1(t), \\ \Omega_2 &= -\frac{i}{\hbar} \int_{-\infty}^{+\infty} \int_{-\infty}^{+\infty} dt_1 dt_2 [V_1(t_1), V_1(t_2)], \\ \Omega_3 &= -\frac{i}{\hbar} \int_{-\infty}^{+\infty} \int_{-\infty}^{+\infty} dt_1 dt_2 \int_{-\infty}^{+\infty} dt_3 (\{V_1(t_1), [V_1(t_2), V_1(t_3)] \\ &\quad + V_1(t_3), [V_1(t_2), V_1(t_1)]\}). \end{aligned} \quad (\text{A5})$$

We assume that only Ω_1 contributes to the resulting scattering matrix, and we neglect all other contributions. We will justify this assumption below. Consequently, the scattering matrix has the following form,

$$U = e^{-i(gbS_+ + g^*b^\dagger S_-)}, \quad (\text{A6})$$

where $b = e^{-i\omega_0 \frac{z}{v}}$, $b^\dagger = e^{i\omega_0 \frac{z}{v}}$, and

$$g = \frac{ed_\perp \omega_0}{2\pi\epsilon_0 \hbar v^2} K_1\left(\frac{\omega_0 r_\perp}{v}\right) + i \frac{ed_z \omega_0}{2\pi\epsilon_0 \hbar v^2} K_0\left(\frac{\omega_0 r_\perp}{v}\right). \quad (\text{A7})$$

Now let us justify the assumption discussed after Eq. (S5). If we calculate all other contributions Ω_k , we find that

$$\Omega_k \sim g^k S_\nu, \quad \nu \in (x, y, z). \quad (\text{A8})$$

Thus, if we assume that $|g| \ll 1$, the main contribution is due to Ω_1 .

2. Scattering matrix of the interaction

We introduce the basis of symmetric states of Dicke superradiance, describing an ensemble of indistinguishable two-level atoms. Specifically, denoting by $|g\rangle$ and $|e\rangle$ the single-atom ground and excited states, respectively, the

symmetrized many-body states $|0\rangle, |1\rangle, \dots, |N_a\rangle$ with 0, 1, and N_a excitations, respectively, read

$$\begin{aligned} |0\rangle &\equiv |ggg\dots gg\rangle \\ |1\rangle &\equiv \sqrt{1/N_a}(|egg\dots gg\rangle + |geg\dots gg\rangle + \dots + |ggg\dots ge\rangle) \\ &\dots \\ |N_a\rangle &\equiv |eee\dots ee\rangle, \end{aligned} \quad (\text{A9})$$

We can represent the scattering matrix from Eq. (A6) in terms of symmetric states,

$$\langle m|U|n\rangle \equiv b^{n-m}U_{mn}, \quad (\text{A10})$$

where

$$U_{mn} = \sqrt{m!n!(N-n)!(N-m)!} \sum_{k=0}^n \frac{(-1)^k (\cos |g|)^{N-m+n-2k} (i \sin |g|)^{m-n} (\sin |g|)^{2k}}{k!(n-k)!(m-n+k)!(N-m-k)!}.$$

After tracing out an electron with an initial density matrix $\rho_{\text{initial}}^{mn}$, the superradiant system can be described by

$$\rho_{\text{final}}^{kl} = \sum_{m,n} \langle \psi_{\text{electron}} | b^{(m-k)-(n-l)} | \psi_{\text{electron}} \rangle U_{km} \rho_{\text{initial}}^{mn} U_{nl}^\dagger, \quad (\text{A11})$$

where $|\psi_{\text{electron}}\rangle$ is the wave function of the interacting electron.

3. Gaussian comb electron

We define the Gaussian comb electron as

$$|\psi_{\text{electron}}\rangle = \frac{1}{\sqrt{\text{norm}}} \sum_n e^{i\phi n} e^{-\frac{k^2}{2\sigma^2}} |\psi_n\rangle, \quad (\text{A12})$$

where $|\psi_n\rangle = \int dE e^{-\frac{(E-E_n)^2}{2\Delta^2}} |E\rangle$, $\phi \in [0, 2\pi]$ is an arbitrary phase, and norm is the normalization of the wave function. We note that $E_n = E_0 + n\hbar\omega$, where ω is the energy shift between different peaks. It follows that

$$\langle b^k \rangle = \frac{1}{\text{norm}} e^{i\phi k} \sum_{n,m} e^{-\frac{(n^2+m^2)}{2\sigma^2}} e^{-\frac{[\xi k+(n-m+k)]^2}{4\Delta^2}}, \quad (\text{A13})$$

where $\xi = (\omega_0 - \omega)\omega^{-1}$ is the dimensionless difference in frequency between atomic transition ω_0 and electron comb frequency ω . By substituting the Gaussian comb electron in Eq. (A11) it is possible to obtain the atomic density matrix following the interaction with N_e consequent electrons. For this purpose, we need to consequently apply Eq. (A11) N_e times on the initial ground state of the atomic system. In this

way, Eq. (A11) was used to produce the plots in Figs. 2 and 3 of the main text.

4. Average energy of the excitation

The total atomic energy reads

$$\hat{E} = \hbar\omega_0 \sum_i \sigma_+^{(i)} \sigma_-^{(i)} = \sum_i \hat{E}_i.$$

Due to symmetry, the single-particle state of each atom with index i is the same. Thus, $\langle \hat{E} \rangle = N_a \langle \hat{E}_i \rangle = N_a \hbar\omega_0 \text{Tr}_i[\sigma_+^{(i)} \sigma_-^{(i)} \rho_i]$. To compute $\langle \hat{E}_i \rangle$, we need to find the single-particle density matrix of atom i after the interaction with the electrons. To this end, we first write the total density matrix (of all atoms plus one electron) after their interaction, namely,

$$\rho_{\text{total,post}} = U \rho_{\text{total,pre}} U^\dagger.$$

The single-particle density matrix of the i th atom after the interaction with one electron is obtained by tracing out everything else, namely,

$$\rho_{i,\text{post}} = \text{Tr}_{\text{atoms except } i} [\text{Tr}_{\text{electron}} (U \rho_{\text{total,pre}} U^\dagger)].$$

While this expression appears complicated, it is linear, and can thus be written as

$$\begin{pmatrix} \rho_i^{00} \\ \rho_i^{01} \\ \rho_i^{10} \\ \rho_i^{11} \end{pmatrix}_{\text{post}} = M \begin{pmatrix} \rho_i^{00} \\ \rho_i^{01} \\ \rho_i^{10} \\ \rho_i^{11} \end{pmatrix}_{\text{pre}},$$

where the matrix M needs to be found. Matrix M is the same as if the electron would interact only with i th atom, since the entanglement and collective effects do not alter the energy of the excitation. Thus, M reads

$$M = \begin{pmatrix} \cos^2 |g| & i\langle b \rangle \sin |g| \cos |g| & -i\langle b \rangle^* \sin |g| \cos |g| & \sin^2 |g| \\ i\langle b \rangle^* \sin |g| \cos |g| & \cos^2 |g| & \langle b^2 \rangle^* \sin^2 |g| & -i \sin |g| \cos |g| \langle b \rangle^* \\ -i\langle b \rangle \sin |g| \cos |g| & \langle b^2 \rangle \sin^2 |g| & \cos^2 |g| & i\langle b \rangle \sin |g| \cos |g| \\ \sin^2 |g| & -i\langle b \rangle \sin |g| \cos |g| & i\langle b \rangle^* \sin |g| \cos |g| & \cos^2 |g| \end{pmatrix}.$$

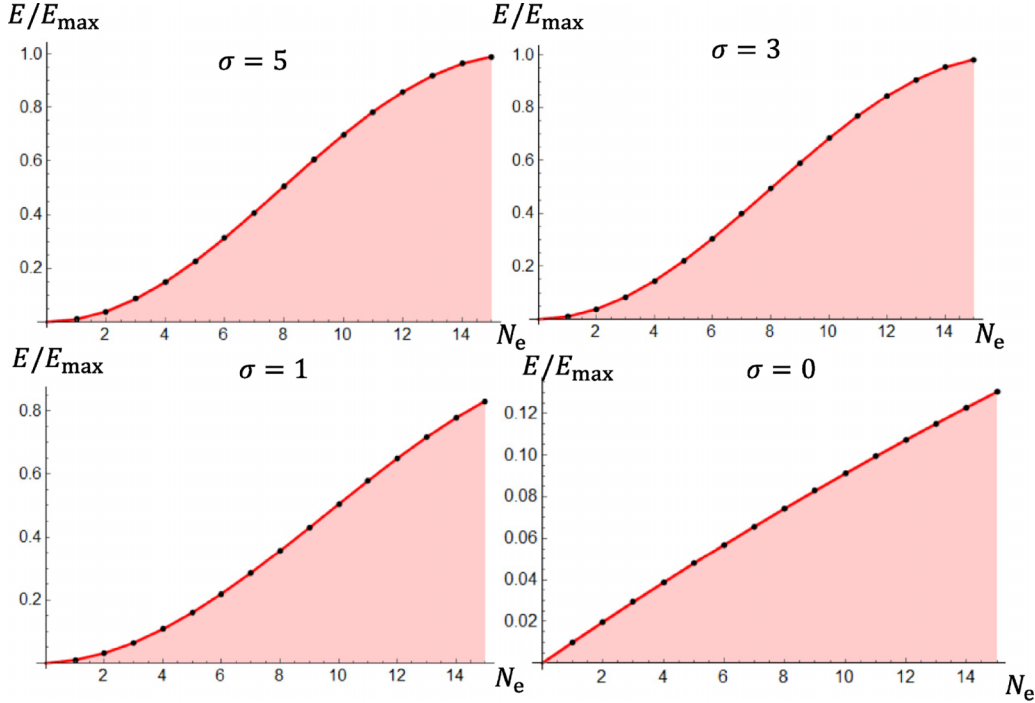


FIG. 6. The comparison of the numerically calculated average excitation energy (red line) as a function of electrons' number N_e and analytically obtained average energy (red line) according to Eq. (A13) for different σ of the electron comb. The calculations show that the analytical formula completely coincides with numerics. The energy is normalized to $N_{\max} = N_a \hbar \omega_0$.

Crucially, M does not depend on the state of the atoms (the quantities $\langle b \rangle$ and $\langle b^2 \rangle$ only depend on the electron). The linear map can thus be iterated to account for the sequential interaction with N_e electrons. Considering atoms initially in their ground state, we thus find

$$\begin{pmatrix} \rho_f^{00} \\ \rho_f^{01} \\ \rho_f^{10} \\ \rho_f^{11} \end{pmatrix} = M^{N_e} \begin{pmatrix} 1 \\ 0 \\ 0 \\ 0 \end{pmatrix},$$

which can be solved exactly upon diagonalizing M . The energy then reads $\langle E \rangle = N_a \hbar \omega_0 \rho_f^{11}$. Namely, in the case of the zero comb's phase (i.e., $\phi = 0$ and $\langle b \rangle = \langle b^* \rangle$):

$$\langle E \rangle = N_a \frac{(\lambda_+^{N_e} - \lambda_-^{N_e})(1 - \langle b^2 \rangle) \sin |g| - (\lambda_+^{N_e} + \lambda_-^{N_e} - 2) \sqrt{(1 - \langle b^2 \rangle)^2 \sin^2 |g| - 16 \langle b \rangle^2 \cos^2 |g|}}{4 \sqrt{(1 - \langle b^2 \rangle)^2 \sin^2 |g| - 16 \langle b \rangle^2 \cos^2 |g|}},$$

$$\lambda_{\pm} = \frac{1}{2} (3 \cos^2 |g| - 1 - \langle b^2 \rangle \sin^2 |g| \pm \sin |g| \sqrt{(1 - \langle b^2 \rangle)^2 \sin^2 |g| - 16 \langle b \rangle^2 \cos^2 |g|}). \quad (\text{A14})$$

As sanity check we calculate the average energy according to analytical equation (A14) and according to the numerical procedure defined in Eq. (A11). The results are the same as shown in Fig. 6.

5. Emission from the excited system

We calculate the emission in two sequential steps: (1) We calculate the atomic density matrix after the interaction with N_e electrons according to Eq. (A11); (2) then we use this density matrix as the initial condition $\rho(0)$ for Dicke superradiance. $\rho(0)$ is found as the postinteraction atomic density matrix using Eq. (A11). The time evolution of the atomic density matrix during superradiance is given by the following equation [35],

$$\frac{d\rho^{mn}(t)}{dt} = -\Gamma/2 [m(N_a - m + 1) + n(N_a - n + 1)] \rho^{mn}(t) + \Gamma \sqrt{(m+1)(N_a - m)(n+1)(N_a - n)} \rho^{(m+1)(n+1)}(t), \quad (\text{A15})$$

where Γ is the rate of spontaneous emission of an individual atom and N_a is the number of atoms. The emission intensity is obtained through energy conservation as $I = -\hbar \omega_0 \sum_{m=0}^N m \frac{d\rho^{mm}(t)}{dt}$.

Specifically, the intensities in Figs. 1(c) and 1(d) of the main text are calculated using Eqs. (A11) and (A13). We also calculate the Wigner functions of the emitted light using the connection between atomic and emitted light correlations derived by Bonifacio *et al.* [36]:

$$\langle a^{\dagger m} a^n \rangle \sim \langle S_+^m S_-^n \rangle. \quad (\text{A16})$$

Equation (A16) gives the ring-shaped Wigner function for a Gaussian electron with $\sigma \ll 1$ and the coherent-state Wigner function for $\sigma \sim 3$, as displaced in Figs. 1(c) and 1(d), respectively.

For comparison, we also calculate the emission from a nonsuperradiant system, which is displayed in Figs. 1(a) and 1(b). In this case, the intensity of emission can be described as the emission of a single atom multiplied by the number of atoms N_a . Thus, we need to solve Eqs. (A11) and (A13) for $N_a = 1$ and then multiply the resulting intensity by the actual number of atoms N_a . The Wigner functions in Figs. 1(a) and 1(b) are thermal, since we assume the atoms to be in equilibrium and independent of each other.

-
- [1] D. B. Williams and C. B. Carter, The transmission electron microscope, in *Transmission Electron Microscopy* (Springer, Berlin, 1996), pp. 3–17.
- [2] F. J. G. De Abajo, Optical excitations in electron microscopy, *Rev. Mod. Phys.* **82**, 209 (2010).
- [3] A. Polman, M. Kociak, and F. J. García de Abajo, Electron-beam spectroscopy for nanophotonics, *Nat. Mater.* **18**, 1158 (2019).
- [4] B. Barwick, D. J. Flannigan, and A. H. Zewail, Photon-induced near-field electron microscopy, *Nature (London)* **462**, 902 (2009).
- [5] A. Feist, K. E. Echternkamp, J. Schauss, S. V. Yalunin, S. Schäfer, and C. Ropers, Quantum coherent optical phase modulation in an ultrafast transmission electron microscope, *Nature (London)* **521**, 200 (2015).
- [6] Y. Morimoto and P. Baum, Diffraction and microscopy with attosecond electron pulse trains, *Nat. Phys.* **14**, 252 (2018).
- [7] B. J. McMorrán, A. Agrawal, I. M. Anderson, A. A. Herzing, H. J. Lezec, J. J. McClelland, and J. Unguris, Electron vortex beams with high quanta of orbital angular momentum, *Science* **331**, 192 (2011).
- [8] V. Grillo, G. C. Gazzadi, E. Karimi, E. Mafakheri, R. W. Boyd, and S. Frabboni, Highly efficient electron vortex beams generated by nanofabricated phase holograms, *Appl. Phys. Lett.* **104**, 43109 (2014).
- [9] S. M. Lloyd, M. Babiker, G. Thirunavukkarasu, and J. Yuan, Electron vortices: Beams with orbital angular momentum, *Rev. Mod. Phys.* **89**, 035004 (2017).
- [10] V. Myroshnychenko, J. Nelayah, G. Adamo, N. Geuquet, J. Rodríguez-Fernández, I. Pastoriza-Santos, K. F. MacDonald, L. Henrard, L. M. Liz-Marzán, N. I. Zheludev *et al.*, Plasmon spectroscopy and imaging of individual gold nanodecahedra: A Combined optical microscopy, cathodoluminescence, and electron energy-loss spectroscopy study, *Nano Lett.* **12**, 4172 (2012).
- [11] B. G. Yacobi and D. B. Holt, *Cathodoluminescence Microscopy of Inorganic Solids* (Springer Science & Business Media, Berlin, 2013).
- [12] S. Meuret, L. H. G. Tizei, T. Cazimajou, R. Bourrellier, H. C. Chang, F. Treussart, and M. Kociak, Photon bunching in cathodoluminescence, *Phys. Rev. Lett.* **114**, 197401 (2015).
- [13] M. Kociak and L. F. Zagonel, Cathodoluminescence in the scanning transmission electron microscope, *Ultramicroscopy* **176**, 112 (2017).
- [14] S. Zheng, J.-K. So, F. Liu, Z. Liu, N. Zheludev, and H. J. Fan, Giant enhancement of cathodoluminescence of monolayer transitional metal dichalcogenides semiconductors, *Nano Lett.* **17**, 6475 (2017).
- [15] D. Cortecchia, K. C. Lew, J.-K. So, A. Bruno, and C. Soci, Cathodoluminescence of self-organized heterogeneous phases in multidimensional perovskite thin films, *Chem. Mater.* **29**, 10088 (2017).
- [16] M. Manceau, K. Y. Spasibko, G. Leuchs, R. Filip, and M. V. Chekhova, Indefinite-mean Pareto photon distribution from amplified quantum noise, *Phys. Rev. Lett.* **123**, 123606 (2019).
- [17] A. Gover and A. Yariv, Free-electron-bound-electron resonant interaction, *Phys. Rev. Lett.* **124**, 064801 (2020).
- [18] D. Rätzel, D. Hartley, O. Schwartz, and P. Haslinger, Controlling quantum systems with modulated electron beams, *Phys. Rev. Res.* **3**, 023247 (2021).
- [19] B. Zhang, D. Ran, R. Ianculescu, A. Friedman, J. Scheuer, A. Yariv, and A. Gover, Quantum wave-particle duality in free-electron-bound-electron interaction, *Phys. Rev. Lett.* **126**, 244801 (2021).
- [20] R. Ruimy, A. Gorlach, C. Mechel, N. Rivera, and I. Kaminer, Toward atomic-resolution quantum measurements with coherently shaped free electrons, *Phys. Rev. Lett.* **126**, 233403 (2021).
- [21] Z. Zhao, X.-Q. Sun, and S. Fan, Quantum entanglement and modulation enhancement of free-electron-bound-electron interaction, *Phys. Rev. Lett.* **126**, 233402 (2021).
- [22] F. J. G. De Abajo and V. Di Giulio, Optical excitations with electron beams: Challenges and opportunities, *ACS Photonics* **8**, 945 (2021).
- [23] A. Karnieli, N. Rivera, A. Arie, and I. Kaminer, The coherence of light is fundamentally tied to the quantum coherence of the emitting particle, *Sci. Adv.* **7**, eabf8096 (2021).
- [24] O. Kfir, V. Di Giulio, F. J. G. de Abajo, and C. Ropers, Optical coherence transfer mediated by free electrons, *Sci. Adv.* **7**, eabf6380 (2021).
- [25] V. Di Giulio, O. Kfir, C. Ropers, and F. J. de Abajo, Modulation of cathodoluminescence emission by interference with external light, *ACS Nano* **15**, 7290 (2021).
- [26] F. J. Garcia de Abajo, E. J. C. Dias, and V. Di Giulio, Complete excitation of discrete quantum systems by single free electrons, *Phys. Rev. Lett.* **129**, 093401 (2022).
- [27] J. S. Nodvick and D. S. Saxon, Suppression of coherent radiation by electrons in a synchrotron, *Phys. Rev.* **96**, 180 (1954).
- [28] F. C. Michel, Intense coherent submillimeter radiation in electron storage rings, *Phys. Rev. Lett.* **48**, 580 (1982).
- [29] A. Gover, F. V. Hartemann, G. P. Le Sage, N. C. Luhmann, Jr., R. S. Zhang, and C. Pellegrini, Time and frequency domain

- analysis of superradiant coherent synchrotron radiation in a waveguide free-electron laser, *Phys. Rev. Lett.* **72**, 1192 (1994).
- [30] J. Urata, M. Goldstein, M. F. Kimmitt, A. Naumov, C. Platt, and J. E. Walsh, Superradiant Smith-Purcell emission, *Phys. Rev. Lett.* **80**, 516 (1998).
- [31] A. S. Gilmour, *Klystrons, Traveling Wave Tubes, Magnetrons, Crossed-Field Amplifiers, and Gyrotrons* (Artech House, Boston, 2011).
- [32] C. Pellegrini, A. Marinelli, and S. Reiche, The physics of x-ray free-electron lasers, *Rev. Mod. Phys.* **88**, 015006 (2016).
- [33] A. Gover, R. Ianconescu, A. Friedman, C. Emma, N. Sudar, P. Musumeci, and C. Pellegrini, Superradiant and stimulated-superradiant emission of bunched electron beams, *Rev. Mod. Phys.* **91**, 035003 (2019).
- [34] R. H. Dicke, Coherence in spontaneous radiation processes, *Phys. Rev.* **93**, 99 (1954).
- [35] M. Gross and S. Haroche, Superradiance: An essay on the theory of collective spontaneous emission, *Phys. Rep.* **93**, 301 (1982).
- [36] R. Bonifacio, P. Schwendimann, and F. Haake, Quantum statistical theory of superradiance. I, *Phys. Rev. A* **4**, 302 (1971).
- [37] R. Bonifacio, P. Schwendimann, and F. Haake, Quantum statistical theory of superradiance. II, *Phys. Rev. A* **4**, 854 (1971).
- [38] R. Brito, V. Cardoso, and P. Pani, *Superradiance* (Springer, Berlin, 2020).
- [39] H. Witek, V. Cardoso, A. Ishibashi, and U. Sperhake, Superradiant instabilities in astrophysical systems, *Phys. Rev. D* **87**, 043513 (2013).
- [40] G. Rainò, M. A. Becker, M. I. Bodnarchuk, R. F. Mahrt, M. V. Kovalenko, and T. Stöferle, Superfluorescence from lead halide perovskite quantum dot superlattices, *Nature (London)* **563**, 671 (2018).
- [41] R. Ruimy, A. Gorlach, G. Baranes, and I. Kaminer, Superradiant electron energy loss spectroscopy, *Nano Lett.* **23**, 779 (2023).
- [42] O. Reinhardt, A. Gorlach, and I. Kaminer, Superradiant cathodoluminescence, in *2021 Conference on Lasers and Electro-Optics (CLEO) (Optica Publishing Group, Washington, DC, 2021)*, pp. 1–2.
- [43] S. T. Park, M. Lin, and A. H. Zewail, Photon-induced near-field electron microscopy (PINEM): Theoretical and experimental, *New J. Phys.* **12**, 123028 (2010).
- [44] K. E. Priebe, C. Rathje, S. V. Yalunin, T. Hohage, A. Feist, S. Schäfer, and C. Ropers, attosecond electron pulse trains and quantum state reconstruction in ultrafast transmission electron microscopy, *Nat. Photonics* **11**, 793 (2017).
- [45] G. M. Vanacore, I. Madan, G. Berruto, K. Wang, E. Pomarico, R. J. Lamb, D. McGrouther, I. Kaminer, B. Barwick, F. J. García de Abajo, and F. Carbone, Attosecond coherent control of free-electron wave functions using semi-infinite light fields, *Nat. Commun.* **9**, 2694 (2018).
- [46] N. Talebi, Strong interaction of slow electrons with near-field light visited from first principles, *Phys. Rev. Lett.* **125**, 080401 (2020).
- [47] D. Cesar, A. Anakru, S. Carbajo, J. Duris, P. Franz, S. Li, N. Sudar, Z. Zhang, and A. Marinelli, Electron beam shaping via laser heater temporal shaping, *Phys. Rev. Accel. Beams* **24**, 110703 (2021).
- [48] R. Shiloh, T. Chlouba, and P. Hommelhoff, Quantum-coherent light-electron interaction in a scanning electron microscope, *Phys. Rev. Lett.* **128**, 235301 (2022).
- [49] J. D. Jackson, *Classical Electrodynamics*, 3rd ed. (John Wiley & Sons, New York, 1998).
- [50] W. Magnus, On the exponential solution of differential equations for a linear operator, *Commun. Pure Appl. Math.* **7**, 649 (1954).
- [51] Y. Pan and A. Gover, Spontaneous and stimulated emissions of a preformed quantum free-electron wave function, *Phys. Rev. A* **99**, 052107 (2019).
- [52] R. Dahan, S. Nehemia, M. Shentcis, O. Reinhardt, Y. Adiv, X. Shi, O. Be'er, M. H. Lynch, Y. Kurman, K. Wang, and I. Kaminer, Resonant phase-matching between a light wave and a free-electron wavefunction, *Nat. Phys.* **16**, 1123 (2020).
- [53] O. Reinhardt and I. Kaminer, Theory of shaping electron wavepackets with light, *ACS Photonics* **7**, 2859 (2020).
- [54] S. V. Yalunin, A. Feist, and C. Ropers, Tailored high-contrast attosecond electron pulses for coherent excitation and scattering, *Phys. Rev. Res.* **3**, L032036 (2021).
- [55] G. Baranes, R. Ruimy, A. Gorlach, and I. Kaminer, Free electrons can induce entanglement between photons, *npj Quantum Inf.* **8**, 1 (2022).
- [56] Y. Adiv, K. Wang, R. Dahan, P. Broaddus, Y. Miao, D. Black, K. Leedle, R. L. Byer, O. Solgaard, R. J. England *et al.*, Quantum nature of dielectric laser accelerators, *Phys. Rev. X* **11**, 041042 (2021).
- [57] Y. Pan, B. Zhang, and A. Gover, Anomalous photon-induced near-field electron microscopy, *Phys. Rev. Lett.* **122**, 183204 (2019).
- [58] A. Pizzi, A. Gorlach, N. Rivera, A. Nunnenkamp, and I. Kaminer, Quantum optics in strongly-driven many-body systems, in *2021 Conference on Lasers and Electro-Optics (CLEO) (Optica Publishing Group, Washington, DC, 2021)*, pp. 1–2.
- [59] G. Baranes, A. Gorlach, R. Ruimy, M. Faran, A. Pizzi, and I. Kaminer, Generating quantum light: New prospects from superradiance, in *CLEO: QELS Fundamental Science (Optica Publishing Group, Washington, DC, 2022)*, pp. FM3B-4.
- [60] M. Scheibner, T. Schmidt, L. Worschech, A. Forchel, G. Bacher, T. Passow, and D. Hommel, Superradiance of quantum dots, *Nat. Phys.* **3**, 106 (2007).
- [61] R. J. England, R. J. Noble, K. Bane, D. H. Dowell, C.-K. Ng, J. E. Spencer, S. Tantawi, Z. Wu, R. L. Byer, E. Peralta, K. Soong, C.-M. Chang, B. Montazeri, S. J. Wolf, B. Cowan, J. Dawson, W. Gai, P. Hommelhoff, Y.-C. Huang, C. Jing *et al.*, Dielectric laser accelerators, *Rev. Mod. Phys.* **86**, 1337 (2014).
- [62] R. Dahan, A. Gorlach, U. Haeusler, A. Karnieli, O. Eyal, P. Yousefi, M. Segev, A. Arie, G. Eisenstein, P. Hommelhoff, and I. Kaminer, Imprinting the quantum statistics of photons on free electrons, *Science* **373**, eabj7128 (2021).
- [63] J.-W. Henke, A. S. Raja, A. Feist, G. Huang, G. Arend, Y. Yang, J. Kappert, R. N. Wang, M. Möller, J. Pan *et al.*, Integrated photonics enables continuous-beam electron phase modulation, *Nature (London)* **600**, 653 (2021).
- [64] A. Feist, G. Huang, G. Arend, Y. Yang, J.-W. Henke, A. S. Raja, F. J. Kappert, R. N. Wang, H. Lourenço-Martins, Z. Qiu *et al.*, Cavity-mediated electron-photon pairs, *Science* **377**, 777 (2022).
- [65] A. Ryabov, J. W. Thurner, D. Nabben, M. V. Tsarev, and P. Baum, Attosecond metrology in a continuous-beam transmission electron microscope, *Sci. Adv.* **6**, eabb1393 (2020).